Environmental Research 290 (2026) 123423

Contents lists available at ScienceDirect

Environmental Research

journal homepage: www.elsevier.com/locate/envres

Quantifying the impact of vegetation greenness change on surface urban heat islands across 133 major cities of China

Rui Yao [a,*], Zhihao Zhang [a], Wenjie Li [a], Hao Li [a], Shiya Zhu [a], Hongji Zhu [a], Chuan Wang [a], Dewei Luo [b], Ying Yang [b], Junli Li [c], Weitao Han [d,e], Xin Huang [f]

[a] College of Resource Environment and Tourism, Hubei University of Arts and Science, Xiangyang, 441053, China
[b] Xiangyang Ecological Environment Monitoring Center, Department of Ecology and Environment of Hubei Province, Xiangyang, 441000, China
[c] School of Resources and Environment, Anhui Agricultural University, Hefei, 230036, China
[d] College of Outstanding Engineers, China University of Geosciences, Wuhan, 430074, China
[e] Hebei Provincial Administration of Surveying, Mapping and Geoinformation, Shijiazhuang, 050031, China
[f] School of Remote Sensing and Information Engineering, Wuhan University, Wuhan, 430079, China

ARTICLE INFO

Keywords:
Remote sensing
Vegetation
Urbanization
Land surface temperature
Surface urban heat island

ABSTRACT

Research on the long-term impacts of vegetation greenness changes on surface urban heat islands (SUHIs) remains limited, with a lack of quantitative assessments. In this study, we proposed a method to quantify the impacts of vegetation greenness changes on the SUHI effect, and assessed their impacts on SUHI intensity and area across 133 major Chinese cities from 2000 to 2023. The results showed that land surface temperature, SUHI intensity and SUHI area increased significantly ($p < 0.05$) in most cities. The proposed method achieved high accuracy. The MAEs for predicted LST were 0.637 °C and 0.358 °C for SDs and SNs, respectively. The predicted LST trend slopes ranged from 0.134 to 0.172 °C/decade for SDs and from 0.067 to 0.073 °C/decade for SNs. The cooling effect of vegetation greenness changes was more pronounced in rural areas than in urban areas, which leads to an increase in the intensity and area of SUHIs. Finally, vegetation greenness changes had a smaller effect on SUHI area (contribution <20 %) than on SUHI intensity (contribution >30 %) during summer days.

1. Introduction

Urbanization is progressing at an unprecedented rate, with specific manifestations such as the expansion of urban areas (Ren et al., 2022) and the increase in urban population (Li et al., 2020). Urbanization can have a series of impacts on the environment, one of which is the well-known urban heat island (UHI) effect—a phenomenon where cities experience higher temperatures than surrounding rural areas due to heat-absorbing infrastructure, reduced vegetation coverage, and human activities (Oke, 1973; Robbiati et al., 2022; Rao et al., 2025; Wang et al., 2025). The UHI effect leads to increased natural mortality (Yuan et al., 2024), reduced thermal comfort for residents (Roshan et al., 2022; Donateo et al., 2023), heightened energy demands for cooling (Hashemi et al., 2024), and disrupted ecological patterns for wildlife and vegetation (Blumstein et al., 2025; Jambhekar et al., 2025). Given these wide-ranging consequences, a precise assessment of UHI spatiotemporal patterns and their driving mechanisms is crucial for developing effective mitigation strategies and guiding sustainable urban development.

Remote sensing can measure land surface temperature (LST); therefore, the UHI detected by this method is referred to as the surface UHI (SUHI) (Voogt and Oke, 2003). Remote sensing has become a powerful tool for SUHI monitoring, because it offers distinct advantages over conventional ground-based meteorological observations, including easier data acquisition, lower monitoring costs, and extensive spatial coverage (Zhou et al., 2019; Chakraborty and Qian, 2024). Over the past few decades, extensive studies have employed remote sensing to analyze SUHI dynamics (Lai et al., 2021; Zhou et al., 2022; Fang et al., 2023; Yang et al. 2023, 2024; Li et al., 2024b; Lu et al., 2024; Zhao et al., 2024). These studies have revealed an aggravating trend of SUHI, particularly in rapidly urbanizing regions such as China and other developing countries (Yao et al., 2021; Li et al., 2022; Islam et al., 2024; Liu et al., 2025).

Numerous studies based on remote sensing and other technologies have shown that vegetation is one of the most important factors influencing the SUHI effect (Peng et al., 2011; Zhou et al., 2019; Li et al., 2024a; Yang et al., 2025). This can be attributed to two key thermal

* Corresponding author. College of Resource Environment and Tourism, Hubei University of Arts and Science, Xiangyang, 441053, China.
E-mail address: yaorui123@hbuas.edu.cn (R. Yao).

https://doi.org/10.1016/j.envres.2025.123423
Received 12 September 2025; Received in revised form 12 November 2025; Accepted 24 November 2025
Available online 24 November 2025

regulation processes: (1) evapotranspiration, which reduces the temperatures through latent heat flux, and (2) canopy shading, which intercepts solar radiation before it heats impervious surfaces (Yang et al., 2025; Zhao et al., 2025). The progressive loss of vegetative cover due to urban expansion directly contributes to elevated temperatures by reducing natural cooling mechanisms (Zhou et al., 2019). In addition, strategic urban greening has been demonstrated as one of the most effective nature-based solutions for UHI mitigation (Li et al., 2024a; Xu et al., 2024).

However, the impacts of long-term vegetation greenness changes in both urban and rural areas on the SUHI effect are poorly understood, with a lack of quantitative assessments. While some studies have revealed temporal and spatial correlations between SUHIs and vegetation (Cui et al., 2021; Liu et al., 2023b; Raj and Yun, 2024), they did not quantify the magnitude of vegetation's impact. Chen et al. (2021) and Wu et al. (2024) quantified the impacts of vegetation greenness change on the SUHI effect of the world and China, respectively, but reached contradictory conclusions: Chen et al. (2021) attributed rising SUHI intensity partly to urban-rural disparities in leaf area index trends, whereas Wu et al. (2024) argued that vegetation greenness changes mitigated SUHIs by cooling urban areas while warming rural ones. Furthermore, prior research has focused predominantly on SUHI intensity, neglecting SUHI area—another critical metric of the SUHI effect.

To address these gaps, this study systematically quantified the impact of long-term vegetation greenness changes on SUHI dynamics. We proposed a novel machine learning-based method to assess vegetation's impact. The accuracy of this method was validated through ten-fold cross-validation. Applying this approach to 133 major Chinese cities for all years between 2000 and 2023, we analyzed impacts of vegetation greenness change on both SUHI intensity and area. The structure of this paper is organized as follows. Section 2 describes the study area and datasets. Section 3 details the methodology. Section 4 presents the main results, followed by discussions in Section 5. Finally, Section 6 concludes the paper.

2. Study area and data

2.1. Study area

China, the world's second most populous country and third-largest by land area (Fig. S1), encompasses approximately 9.6 million square kilometers of remarkably diverse geography. Spanning subtropical to temperate zones, the country exhibits striking climatic variations: frigid winters and hot summers in the northeast, arid/semi-arid conditions in the northwest, and humid subtropical monsoons along the southeastern coast. This vast territory features dramatic topographical contrasts, including the fertile North China Plain, the towering Himalayas, the expansive Taklimakan Desert, and the agriculturally vital Yangtze and Yellow River basins. Land cover is predominantly characterized by forests, grasslands, and cultivated areas, reflecting China's crucial role in global agriculture. Recent decades have witnessed unprecedented urbanization, marked by dramatic expansions in both urban population (Song et al., 2021) and built-up areas (Yang and Huang, 2021), which have significantly exacerbated UHI effects nationwide (Yao et al., 2021; Liu et al., 2023a).

A total of 133 cities with areas exceeding 150 km^2 were selected as the study area for this research (Yang et al., 2024; Yao et al., 2024). The specific methodology for city selection is detailed in Section 3.1. These cities are predominantly located in eastern China, particularly in the North China Plain. Most cities across East China fall under the classification of either temperate monsoon or subtropical monsoon climates. These climate types share the defining characteristic of hot and rainy summers, a feature driven by the moist East Asian summer monsoon. Conversely, winters are typically drier and exhibit significant temperature differences between the north and south. The geographical extent of these cities spans from 83.1°E to 126.6°E in longitude and 20.0°N to 47.3°N in latitude, with elevations ranging between 0 and 1125 m above sea level.

2.2. Data

We utilized MODIS MOD11A2 LST data (Version 6.1) spanning 2000–2023, featuring 1000 m spatial resolution and 8-day temporal compositing. The dataset provides both daytime (10:30 a.m.) and nighttime (10:30 p.m.) measurements at local solar time. The accuracy verification of the product revealed that its error was below 1 °C for most homogeneous non-urban regions (Wan, 2014). This product contains some missing values caused by cloud contamination. Before conducting the SUHI research, these missing values were reconstructed by clear-sky LST using the estimation of the temperature difference (ETD) method proposed by Yao et al. (2023a).

Enhanced Vegetation Index (EVI) data were obtained from MODIS MOD13A2 (Version 6.1, 2000–2023), offering 1000 m resolution with 16-day composites. EVI was preferred over NDVI due to its: (1) superior sensitivity to canopy variations in high-biomass regions, and (2) enhanced performance for urban vegetation monitoring (Huete et al., 2002; Zhang et al., 2004). This product contains some low quality values caused by cloud contamination. Before conducting vegetation-related research, the EVI values of pixels other than "good-quality" were removed and reconstructed using the spatial-interannual reconstruction (SIR) method proposed by Yao et al. (2023b).

This study utilized MODIS data due to its significant advantages, including its long time series (from 2000 to the present), high temporal resolution (two satellites collectively observe the Earth four times a day), global coverage, and ease of data accessibility. Terra-derived products (MOD11A2/MOD13A2) were selected over Aqua equivalents (MYD11A2/MYD13A2) due to their longer temporal coverage (February 2000–present vs. July 2002–present). Analysis was restricted to summer months (June–August) because: (1) the heightened public health impacts of extreme summer temperatures compared to other seasons (2) vegetation activity (e.g., transpiration, photosynthesis); peaks during this season.

For land cover characterization, we employed the China Land Cover Dataset (CLCD) (version 3) (Yang and Huang, 2021), which provides annual 30-m resolution maps from 2000 to 2023. This dataset distinguishes nine land cover categories (cropland, forest, shrub, grassland, wetland, water bodies, impervious surfaces, barren land, and snow/ice) with demonstrated high accuracy. Elevation data were derived from the global multi-resolution terrain elevation data 2010 (GMTED2010) (Danielson and Gesch, 2011) at 1 km resolution. Using these elevation data in ArcGIS, we subsequently derived 1 km resolution clear-sky solar radiation data in ArcGIS software.

3. Methods

3.1. Preprocessing

We obtained 30 m resolution impervious surface maps for 2000 and 2023 from the CLCD, which were then aggregated to 1 km resolution by calculating impervious surface proportions to maintain consistency with other datasets. Urban pixels were defined as those with >50 % impervious surface coverage (Imhoff et al., 2010; Zhou et al., 2022; Wu et al., 2024). We do not set the threshold higher to avoid excluding the urban-rural fringe, nor do we set it lower to prevent the selected urban areas from merging and becoming indistinguishable. From these, we selected 133 urban areas exceeding 150 km^2 in 2023 as our study areas (Yang et al., 2024; Yao et al., 2024; Liu et al., 2025). The derived urban areas in 2023 was further categorized into: (1) old urban areas (consistently urban in both 2000 and 2023), and (2) new urban areas (transitioned from non-urban to urban during 2000–2023) (Gui et al., 2019; Wang et al., 2016; Zhou et al., 2025). The reason for categorizing urban areas into these two types is that they generally exhibit different

trends in vegetation greenness and SUHI effects (Gui et al., 2019; Wang et al., 2016). Rural areas were identified by first creating 10–30 km buffers around urban boundaries and excluding any pixels with impervious surface coverage >0 % (Imhoff et al., 2010; Yao et al., 2021; Yang et al., 2024). A buffer zone distance of 10–30 km is appropriate, ensuring that the area is not affected by the SUHI effect from being too close to the city, nor does it exhibit a weak correlation with the city due to excessive distance. Furthermore, we excluded areas with any impervious surface (i.e., >0 %) from the rural definition to eliminate the influence of urbanization and establish reliable rural reference areas.

Note that we retained rural pixels despite significant elevation differences from urban pixels, as well as water pixels, for three reasons.

(1) Although these pixels influence the calculation of the SUHI intensity, they do not affect the calculation of its temporal trend. Retaining these pixels leads to an overestimation of the SUHI intensity. However, since this overestimation is consistent in magnitude across all years, it does not impact the derived trend over time. This has been demonstrated by Yao et al. (2018a).
(2) By retaining pixels with significant elevation differences from cities, we preserve more natural vegetation (e.g., forests, which are typically located in mountainous areas surrounding cities, unlike croplands on plains) in rural areas. In contrast, areas with comparable elevations to urban areas are predominantly plains and covered by croplands. These croplands are subject to substantial human influence, causing greater fluctuations in EVI and LST (Yao et al., 2018a).
(3) If we remove pixels with significant elevation differences from the urban areas as well as water body pixels from the buffer zone, then in some cities, only a very small number of pixels will remain in the buffer. Using a limited number of pixels as rural areas may introduce some uncertainties.

3.2. Analysis of trends in LST, SUHI intensity, SUHI area, EVI, and ΔEVI

SUHI intensity was calculated using Equations (1) and (2), and ΔEVI was calculated using Equations (3) and (4), as follows:

$$SUHI\ intensity_n = LST_n - LST_r \quad (1)$$

$$SUHI\ intensity_o = LST_o - LST_r \quad (2)$$

$$\Delta EVI_n = EVI_n - EVI_r \quad (3)$$

$$\Delta EVI_o = EVI_o - EVI_r \quad (4)$$

where LST_n, LST_o and LST_r are the average LST of all pixels in new urban, old urban and rural areas, respectively. EVI_n, EVI_o and EVI_r are the average EVI of all pixels in new urban, old urban and rural areas, respectively. $SUHI\ intensity_n$ and $SUHI\ intensity_o$ are SUHI intensity in new and old urban areas, respectively. ΔEVI_n and ΔEVI_o are ΔEVI in new and old urban areas, respectively. All calculations were performed separately for each city and for each year.

The SUHI area was calculated using the following steps (Zhang and Wang, 2008; Schwarz et al., 2011; Ward et al., 2016). First, a 10 km buffer area was created around each city boundary, with areas belonging to adjacent cities being excluded. Within these processed urban and buffer areas, pixels exhibiting both an impervious surface proportion >0 % and LST values at least 1 °C higher than surrounding rural areas were identified as SUHI-affected areas, with their cumulative area representing the city's total SUHI area. The 10 km buffer threshold was adopted based on previous research demonstrating that SUHI footprints typically remain within this range (Zhang et al., 2004; Zhou et al., 2015). The 1 °C threshold was selected to account for the <1 °C measurement uncertainty in MODIS LST data (Wan, 2014). Sensitivity analysis of these thresholds (i.e., 10 km and 1 °C) is presented in the discussion section. Note that we opted against using the Gaussian model to calculate the SUHI area (Streutker, 2002), primarily because it often fails to fit SUHI patterns—especially in cities with multi-core SUHI structures (Quan et al., 2014). Linear regression was used to analyze the temporal trends of LST, SUHI intensity and area, EVI, and ΔEVI from 2000 to 2023.

3.3. Quantifying the impacts of vegetation greenness changes on LST and SUHI

The impacts of vegetation greenness changes on LST and SUHI were quantified using a three-stage analytical framework (Fig. 1). First, LST, EVI, elevation, proportion of impervious surface, proportion of water bodies, and clear-sky solar radiation data were extracted from urban areas and their surrounding 30 km buffers. Second, we employed the Cubist machine learning model (Quinlan, 1992), a rule-based regression approach derived from M5 model trees, known for its high predictive accuracy and computational efficiency (Xu et al., 2018; Han et al., 2023). Unlike conventional regression models, Cubist generates multiple rule-based predictive frameworks. In this study, the Cubist model was implemented using the 'Cubist' add-on package (Kuhn and Quinlan, 2024) in R software. There are two parameters in the Cubist model: committees and neighbors. We employed the bootstrap method from the 'caret' add-on package (Kuhn, 2008) in R software to find appropriate settings for these parameters. The two packages used are highly efficient, automatically handling the entire process of parameter selection, model training, and prediction. In our implementation, EVI, elevation, proportion of water bodies, proportion of impervious surface, and solar radiation served as independent variables to predict LST (dependent variable). These five independent variables were selected as predictors due to their strong correlations with LST and demonstrated capacity to enhance LST estimation accuracy (see section 4.2). Please note that both elevation and clear-sky solar radiation are assumed constant over the study period. This is because large-scale topography changes negligibly over decades, and time-series elevation data are unavailable. Meanwhile, clear-sky solar radiation—the radiation received under cloudless conditions—is determined by topography and latitude, which are effectively constant. A relationship between the independent and dependent variables was fitted using the Cubist machine learning model. All data within the city and its surrounding 30 km buffer zone were used to fit this relationship, with each city's data fitted separately for each year. The maximum, average, and minimum sample sizes across the 133 cities were 26,496, 6,983, and 4,816, respectively. Third, we held EVI constant at 2000 levels for 2001–2023, while maintaining the original values of all other independent variables. Using this detrended EVI (with 0/decade trend) along with other independent variables, we generated vegetation-static LST predictions. These predicted values remain unaffected by vegetation greenness changes but are influenced by other factors such as urbanization. In contrast, the observed LST is affected by both vegetation greenness variations and other factors including urbanization. Therefore, the difference between the predicted and observed LST trends represents the impact of vegetation greenness change on LST trends. Consequently, the difference in the SUHI derived from predicted versus observed LST quantifies the specific effects of vegetation greenness changes on SUHIs.

We used two ways to validate the accuracy of this approach.

(1) A crucial component of our methodology involves estimating LST using five independent variables: EVI, elevation, proportion of water bodies, proportion of impervious surface, and clear-sky solar radiation. To ensure the reliability of these estimations, we performed ten-fold cross-validation. The validation procedure consisted of the following steps: (a) all pixels within urban areas and their 30 km buffer zones were randomly partitioned into ten equal subsets; (b) for each validation round, nine subsets were used to train the model while the remaining subset served as

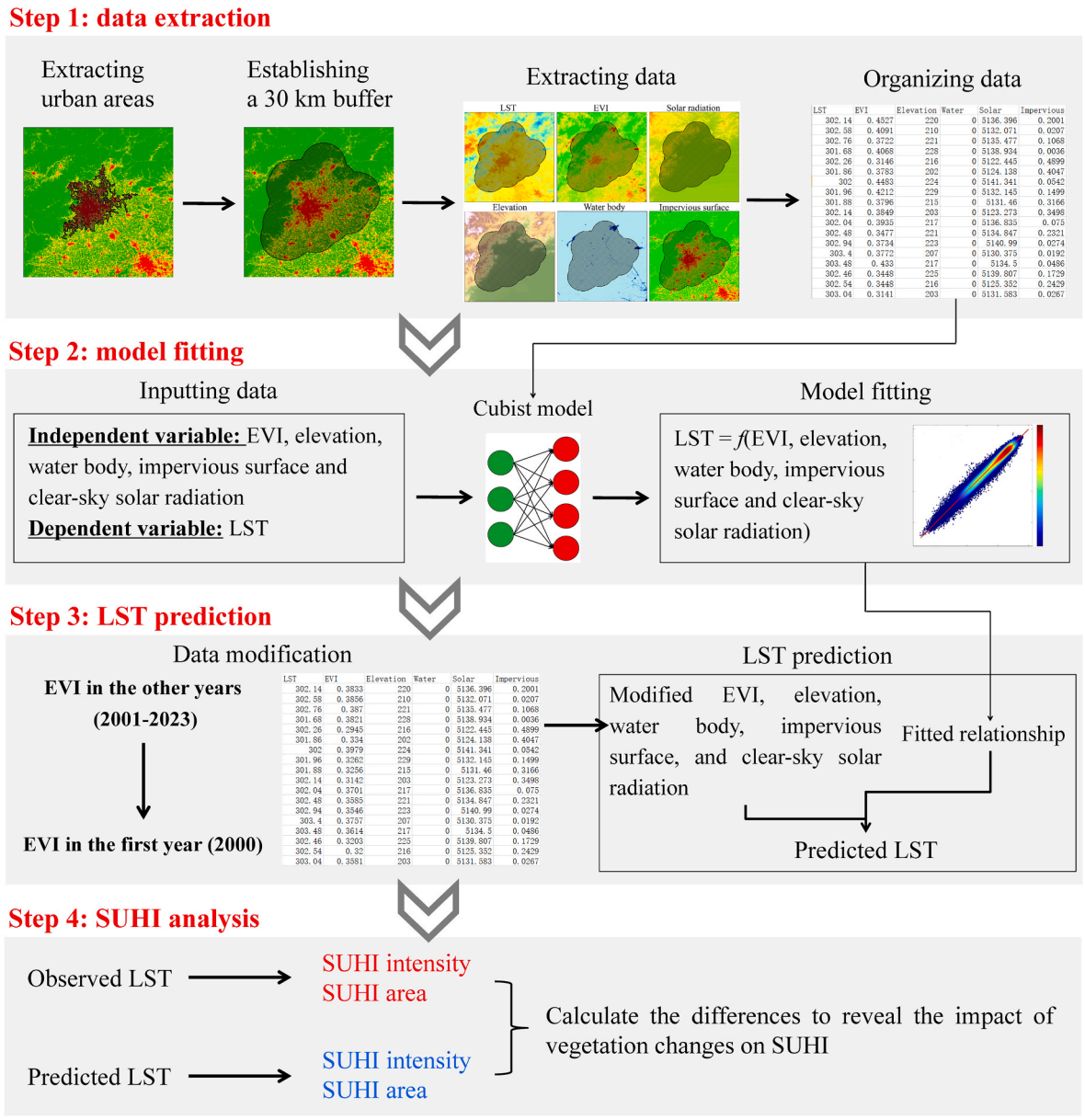

Fig. 1. Flowchart for quantifying the impact of vegetation greenness changes on land surface temperature (LST). EVI: enhanced vegetation index. SUHI: surface urban heat island.

validation data; (c) this rotation process was repeated ten times until each subset had been used exactly once for validation.

(2) In each of the three regions (old urban area, new urban area and rural area) of every city, we identified the 10 % of pixels with EVI trends closest to zero. These pixels were considered unaffected by vegetation greenness changes. The average LST trend of these pixels was defined as the LST trend for the region unaffected by vegetation greenness changes. The accuracy of the proposed method was then determined by comparing this reference trend against the predicted LST trend by the proposed method. Regions with fewer than 100 pixels were excluded from validation.

The first method validated the predicted LST, while the second method validated the predicted LST trend. The mean absolute error (MAE), root mean square error (RMSE), coefficient of determination (R^2), and bias were used to describe the accuracy.

4. Results

4.1. Trends of LST, SUHI intensity, SUHI area, EVI, and ΔEVI

During summer days (SDs) from 2000 to 2023, LST increased in both new and old urban areas across the majority of cities (Figs. 2 and 3, and Table 1). Over half of these cities demonstrated statistically significant ($p < 0.05$) increases. In contrast, LST in rural areas remained relatively constant, showing no significant trends ($p \geq 0.05$) in most cities. During summer nights (SNs), LST increased significantly ($p < 0.05$) in new urban areas, old urban areas and rural areas in nearly all cities. The LST in both old and new urban areas increased at a faster rate than in rural areas, leading to a pronounced upward trend in SUHI intensity. From 2000 to 2023, the average SUHI intensity across 133 cities increased by 0.461 °C/decade and 0.909 °C/decade during SDs in old and new urban areas, respectively (Fig. 3). The increasing rate of SUHI intensity was higher during SDs compared to SNs. Additionally, the SUHI area expanded in most cities over the same period (Fig. 2). On average, the

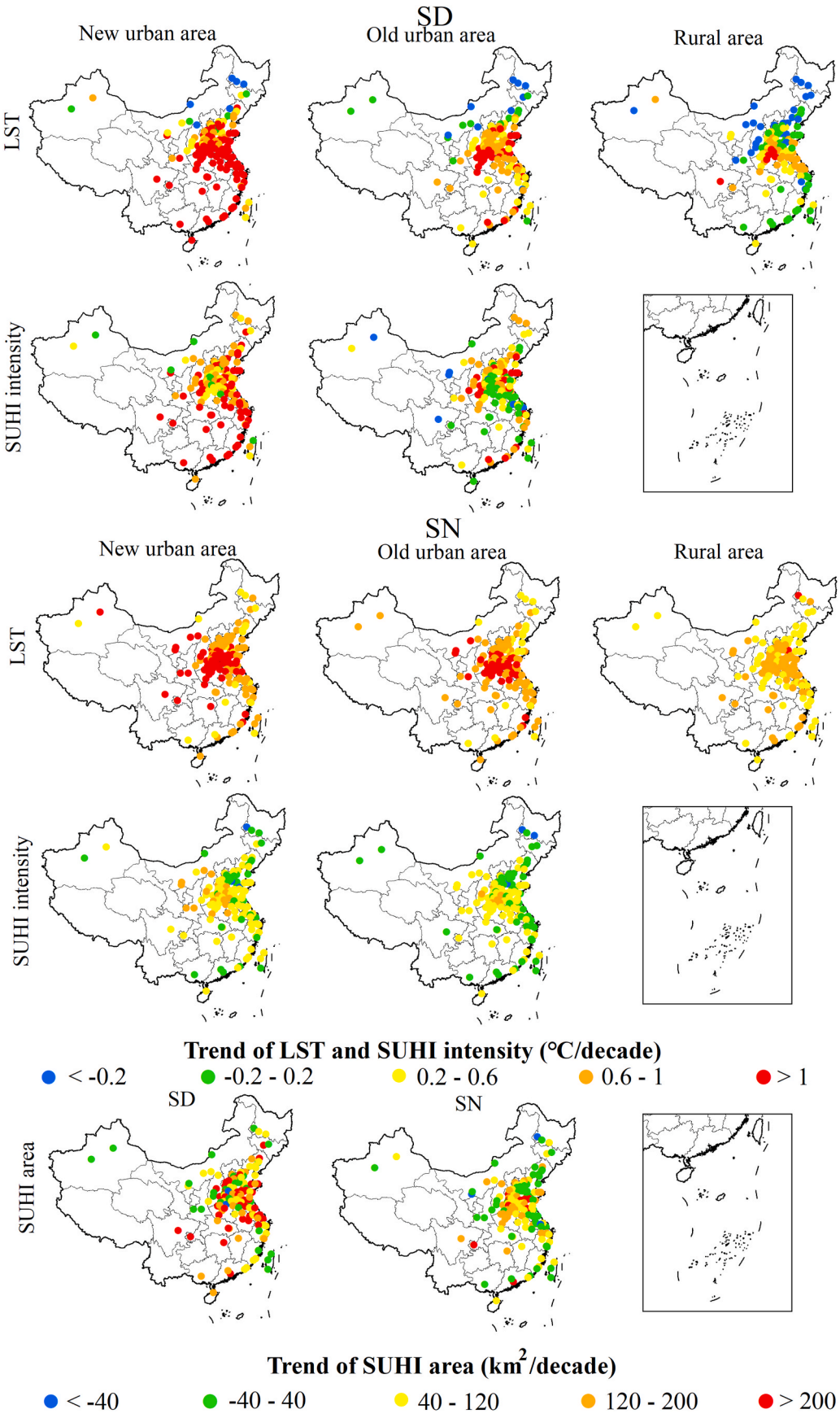

Fig. 2. Spatial distributions of trends of LST, SUHI intensity, and SUHI area. SD: summer day. SN: summer night.

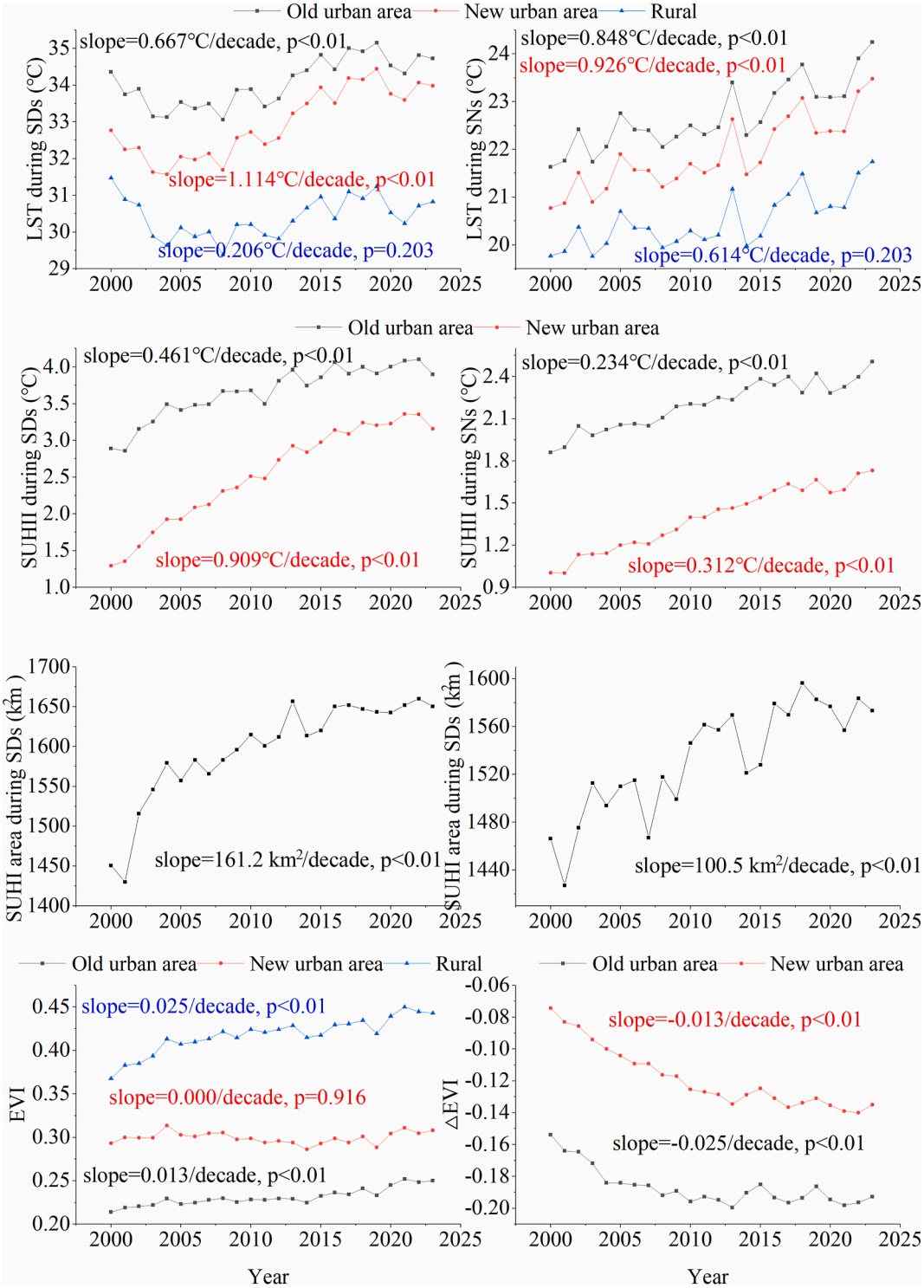

Fig. 3. Interannual variations of LST, SUHI intensity, SUHI area, EVI, and ΔEVI.

SUHI area increased at rates of 161.2 km^2/decade during SDs and 100.5 km^2/decade during SNs across all cities (Fig. 3).

Interannually, while the LST exhibits an overall upward trend, it experienced a temporary decline from 2000 to 2012 (Fig. 3) due to a hiatus in global warming during that period (Kosaka and Xie, 2013). However, LST resumed its upward trend beginning in 2013. Further analysis indicates that these LST trends are similar to the air temperature trends derived from the ERA5-Land reanalysis dataset (Fig. S2). The SUHI intensity increased more rapidly during the first half of the study period and more slowly in the second half, primarily due to a faster decline in ΔEVI in the earlier period compared to the latter (Fig. 3). Spatially, LST trends were relatively lower in Northeast China (Fig. S3), a pattern partially attributable to the high EVI trend slopes of this region (Fig. S4). The trends of SUHI intensity during SDs were relatively high in the new urban areas of Southwest, East, and Central-South China, which aligns with the declining EVI trends observed there. Furthermore, both LST and SUHI intensity increased significantly faster in new urban areas than in old urban areas. For instance, the rate of SUHI intensity increase

Table 1
Number of cities with significant and insignificant trends of LST, SUHI intensity, EVI and ΔEVI. LST: land surface temperature. EVI: enhanced vegetation index. SUHI: surface urban heat island. SD: summer day. SN: summer night.

	LST in new urban area	LST in old urban area	LST in rural area	SUHI intensity in new urban area	SUHI intensity in old urban area
SD					
Significant increasing trend	102	78	39	122	82
Insignificant trend	29	53	88	11	48
Significant decreasing trend	2	2	6	0	3
SN					
Significant increasing trend	128	124	119	100	77
Insignificant trend	5	9	14	30	52
Significant decreasing trend	0	0	0	3	4
	EVI in new urban area	EVI in old urban area	EVI in rural area	ΔEVI in new urban area	ΔEVI in old urban area
Significant increasing trend	34	93	101	2	13
Insignificant trend	57	32	29	21	44
Significant decreasing trend	42	8	3	110	76

on SDs was twice as high in new urban areas (0.909 °C/decade) as in old urban areas (0.462 °C/decade). This disparity arises because: (1) urbanization processes occurred predominantly in new urban areas; and (2) EVI increased significantly in old urban areas but remained stable (trend close to zero) in new urban areas (see next paragraph).

EVI exhibited significant increases in both old urban areas and rural areas across most cities (Fig. S4 and Table 1). When averaged across all cities, EVI increased at rates of 0.013/decade ($p < 0.01$) and 0.025/decade ($p < 0.01$) in old urban areas and rural areas, respectively. However, new urban areas showed a near-zero trend in EVI when averaged over the 133 cities, differing from the other two areas. Further analysis revealed significant regional differences in the EVI trends of new urban areas. The EVI in new urban areas of North, Northeast and Northwest China increased, while it declined in other regions (Fig. S3). Finally, ΔEVI decreased significantly in both new and old urban areas from 2000 to 2023 (Fig. S4).

4.2. Accuracy verification of the proposed method

The proposed method demonstrated satisfactory accuracy (Table 2). The ten-fold cross-validation results showed MAEs of 0.637 °C and 0.358 °C for predicted LST during SDs and SNs, respectively. This performance closely aligns with that of the MODIS LST product, which typically exhibits errors below 1 °C (Wan, 2014). Additionally, the bias in the estimated LST was close to 0 °C. The reduced accuracy during SDs compared to SNs likely stems from higher LST variability and more complex influencing factors during SDs (Yao et al., 2023a). The accuracy for the predicted LST trend was also high: MAE ranged from 0.134 to 0.172 °C/decade on SDs and from 0.067 to 0.073 °C/decade on SNs, while the R^2 exceeded 0.86 in most cases. Such precise estimations are crucial for accurately assessing the impact of vegetation greenness on LST and the SUHI effect.

The four variables—EVI, clear-sky solar radiation, proportion of water bodies, and elevation—all contributed to LST estimation (Table 2). Excluding any of them reduced the estimation accuracy. Among these, EVI had the strongest impact: omitting it increased the MAEs of LST estimation by 0.132 °C during SDs and 0.042 °C during SNs. This is because vegetation reduces daytime LST through evapotranspiration, and lowers nighttime LST by limiting heat storage in the ground during the day (Yao et al., 2018b). Elevation generally exhibits a strong negative correlation with LST—higher elevations correspond to lower LSTs—so including elevation as a variable improves LST estimation precision. Solar radiation significantly influences LST, as intense radiation increases ground heat absorption, thereby raising LST. Water bodies cool daytime LST (due to high heat capacity and evaporation) but warm nighttime LST (due to slower heat release), resulting in a negative correlation during SDs and a positive correlation during SNs with LST. An increase in the proportion of impervious surfaces will raise LST. The first reason is the low evaporation rate of impervious surfaces, which reduces evaporative cooling of the land surface (Arnfield, 2003; Zhou et al., 2019). The second reason is that impervious surfaces have high heat capacity, allowing them to absorb substantial heat during the day and release it slowly at night, which keeps the nighttime LST at a relatively high level (Oke et al., 1991).

4.3. The impacts of vegetation greenness changes on LST and SUHI effect

Changes in vegetation greenness significantly affected LST and the

Table 2
Accuracy of the proposed method. MAE: mean absolute error. RMSE: root mean square error. R^2: coefficient of determination.

Accuracy of predicted LST	Using all five variables	Exclusion of elevation	Exclusion of clear-sky solar radiation	Exclusion of EVI	Exclusion of proportion of water body	Exclusion of proportion of impervious surface
SD						
MAE (°C)	0.637	0.713	0.691	0.769	0.661	0.667
RMSE (°C)	0.867	0.974	0.933	1.062	0.908	0.921
R^2	0.912	0.889	0.898	0.868	0.904	0.901
Bias (°C)	−0.011	−0.007	−0.006	−0.008	−0.010	−0.010
SN						
MAE (°C)	0.358	0.401	0.394	0.400	0.364	0.369
RMSE (°C)	0.487	0.551	0.529	0.541	0.494	0.504
R^2	0.960	0.949	0.953	0.951	0.959	0.957
Bias (°C)	0.005	0.003	0.002	0.003	0.004	0.005
Accuracy of predicted LST trend	SD, old urban area	SD, new urban area	SD, rural area	SN, old urban area	SN, new urban area	SN, rural area
MAE (°C/decade)	0.134	0.172	0.157	0.073	0.068	0.067
RMSE (°C/decade)	0.188	0.225	0.212	0.093	0.088	0.094
R^2	0.939	0.868	0.907	0.920	0.899	0.766
Bias (°C/decade)	0.010	−0.020	0.090	0.040	0.008	−0.013

SUHI effect (Table 3). In old urban areas, the observed and predicted LST trends during SDs were 0.667 °C/decade and 0.771 °C/decade, respectively. Vegetation greening thus reduced LST by 0.104 °C/decade in old urban areas during SDs. The cooling effect of vegetation greenness changes was more pronounced in rural areas, with LST decreasing by 0.292 °C/decade during SDs. Since SUHI intensity equals urban LST minus rural LST, greening in old urban areas weakened SUHI intensity by 0.104 °C/decade, while rural greening enhanced it by 0.292 °C/decade. The overall trend of SUHI intensity in old urban areas was 0.461 °C/decade during SDs. These results indicate that vegetation greening in rural areas contributed substantially to the increase in SUHI intensity. In the new urban areas, the average EVI trend across the 133 cities was close to zero per decade, and its impact on LST during SDs was also nearly 0 °C/decade (Table 3). This contrasts with the decrease in LST observed in old urban and rural areas.

Vegetation greenness changes had weaker impact on the trend of SUHI intensity during SNs than during SDs (Table 3). For example, vegetation greenness changes in old urban areas contributed to LST trends of −0.104 °C/decade during SDs and −0.048 °C/decade during SNs. In addition, the combined impact of vegetation greenness changes in both old urban and rural areas led to an increase in SUHI intensity of 0.188 °C/decade and 0.023 °C/decade during SDs and SNs, respectively. This difference is mainly because evapotranspiration from vegetation occurs predominantly during daytime and thus has a more direct influence on daytime LST (Peng et al., 2011; Song et al., 2025).

Vegetation greenness changes also contributed to an expansion of the SUHI area (Table 3). The observed and predicted SUHI areas during SDs were 161.2 km^2/decade and 143.4 km^2/decade, respectively, indicating that vegetation greenness changes increased the SUHI area by 12.4 %. This occurs primarily because vegetation greening in rural areas significantly reduces rural LST, leading more urban pixels to exceed the LST difference threshold used to define SUHI area. Additional analysis revealed that the estimated trends in SUHI area differ substantially depending on whether the impact of rural vegetation greening is considered (not shown).

5. Discussion

5.1. Impacts of vegetation greenness changes on the SUHI effect

This study reveals a deteriorating thermal environment across Chinese cities, marked by significant increasing trends in LST, SUHI intensity, and SUHI area in most cities. These changes are likely to impose a range of adverse effects on both human populations and ecosystems, warranting greater attention and mitigation efforts.

Our findings indicate that changes in vegetation greenness have contributed to a significant increase in both the intensity and area of SUHIs. This is because the significant greening of rural vegetation has substantially lowered rural LST, whereas the increase in urban vegetation greenness is much less pronounced than in rural areas (Table 3), resulting in a weaker cooling effect in urban areas. Consequently, urban areas are likely to remain highly vulnerable to synergistic warming from ongoing urbanization and climate change. To mitigate this risk, targeted measures to enhance urban vegetation are critically needed.

In this study, vegetation greenness changes had a smaller impact on the trend in SUHI area (contribution <20 %) than on SUHI intensity (contribution >30 %) during SDs (Table 3). This discrepancy can be attributed to the fact that urban core areas—already characterized by elevated LST—are consistently classified within the SUHI area irrespective of vegetation greenness changes.

A detailed comparison between this study and other similar literature is shown in Table S1. Two studies are most closely related to this work. Chen et al. (2021) and Wu et al. (2024) quantified the impacts of vegetation greenness change on the SUHI effect at the global and Chinese scale, respectively. The conclusions of this study align with those of Chen et al. (2021) (that a widening leaf area index gap between urban and rural areas contributes to the increase in SUHI intensity) but differ from the findings of Wu et al. (2024) (that vegetation changes cool urban areas and warm rural areas, thereby attenuating the SUHI intensity). However, the reason for the discrepancy between our conclusions and those of Wu et al. (2024) remains unclear and may be attributable to methodological differences. Additionally, Yao et al. (2019) found that greening reduced the LST in rural areas, and contributed 22.5 % of the increased daytime SUHI intensity. However, this study solely quantified the contribution of rural vegetation greenness changes to the SUHI intensity.

Table 3
Impacts of vegetation greenness changes on trends of LST and SUHI.

LST during SDs (°C/decade)	Old urban area	New urban area	Rural
Observed	0.667	1.114	0.206
Predicted	0.771	1.094	0.498
Impact	−0.104	0.020	−0.292
LST during SNs (°C/decade)	Old urban area	New urban area	Rural
Observed	0.848	0.926	0.614
Predicted	0.897	0.915	0.685
Impact	−0.048	0.011	−0.071
SUHI intensity during SDs (°C/decade)	Old urban area		New urban area
Observed	0.461		0.909
Predicted	0.273		0.596
Impact	0.188		0.313
SUHI intensity during SNs (°C/decade)	Old urban area		New urban area
Observed	0.234		0.312
Predicted	0.212		0.230
Impact	0.023		0.082
SUHI area (km^2/decade)	SDs		SNs
Observed	161.2		100.5
Predicted	143.4		84.7
Impact	17.8		15.8

5.2. Impact of threshold selection on SUHI area calculation

The influence of threshold selection on the calculated SUHI area is illustrated in Fig. S5. Four thresholds were adopted for generating the buffer zones: distances of 5 km, 10 km, and 15 km, as well as a scenario where the buffer area equaled the urban area. For defining the SUHI area, four LST thresholds were used: 0.5 °C, 1 °C, 1.5 °C, and the standard deviation of rural LST. Overall, although the results vary in magnitude depending on the thresholds applied, the key conclusions remain consistent: (1) the predicted-LST-based SUHI areas were smaller than the observed-LST-based results, confirming that vegetation greenness changes have contributed to an expansion of the SUHI area; and (2) the increasing trends of SUHI areas were stronger during SDs than during SNs.

The estimated trend in SUHI area increased with larger distance thresholds. For instance, using a 1 °C LST threshold combined with distance thresholds of 5 km, 10 km, and 15 km yielded SUHI area trends of 109.3 km^2/decade, 161.2 km^2/decade, and 214.0 km^2/decade, respectively, during SDs (Fig. S5). This pattern arises because larger buffers incorporate more pixels influenced by the SUHI effect. Additionally, the SUHI area trend during SDs increased with higher LST thresholds, whereas during SNs, the smallest trend occurred at the maximum LST threshold (1.5 °C). This discrepancy is attributed to the stronger SUHI intensity during SDs compared to SNs. During SNs, a substantial proportion of the urban area exhibits SUHI intensities below 1.5 °C. Therefore, using 1.5 °C as the threshold for SUHI intensity during SNs is somewhat high.

5.3. Contributions and limitations

The contributions of this paper include both methodological and

research content aspects. First, we proposed a machine learning-based method to quantify the impacts of vegetation greenness changes on SUHIs, which has been validated to achieve high accuracy. The MAEs of the method proposed in this study were 0.637 °C and 0.358 °C during SDs and SNs, respectively. However, methods introduced in previous studies lacked validation (Chen et al., 2021; Wu et al., 2024; Yao et al., 2019; Li et al., 2024a). Additionally, this method is relatively simple and holds potential for application in other fields in the future. Second, addressing a current research gap, this study provided a precise quantification of how vegetation greenness changes in both urban and rural areas affect SUHI intensity and area. However, previous studies have focused solely on the single metric of SUHI intensity (Chen et al., 2021; Wu et al., 2024; Yao et al., 2019). The results of this study can improve our understanding of SUHI spatiotemporal dynamics and their interaction with vegetation.

The study has three main limitations. First, it investigates the SUHI based on satellite-measured LST, which is distinct from the atmospheric UHI based on air temperature. The latter is more directly relevant to human health and thermal comfort (Yao et al., 2021). This distinction is underscored by evidence that vegetation's cooling effect is more pronounced on LST than on air temperature (Du et al., 2024). Future work could explore this aspect once high-resolution, long-term gridded air temperature data become available. Second, while the impacts of vegetation greenness change were quantified, the specific biophysical mechanisms—such as the relative contributions of albedo and evapotranspiration—were not explicitly analyzed. Subsequent research could integrate physical models to disentangle these factors. Third, although the accuracy of the MODIS LST product has been verified in some contexts, its performance specifically over urban areas remains unvalidated (Wan, 2014; Duan et al., 2019). Given that this study, along with numerous previous ones, relies on MODIS LST for SUHI research, future studies should prioritize evaluating its accuracy in urban areas.

6. Conclusions

In this study, a novel method was developed to quantify the impacts of vegetation greenness changes on the SUHI effect. The impacts of long-term vegetation dynamics on SUHI intensity and area were systematically analyzed across 133 major Chinese cities from 2000 to 2023.

Results indicate a progressively deteriorating thermal environment in these cities, with significant increasing trends observed in LST, SUHI intensity, and SUHI area across most cities. Notably, LST and SUHI intensity increased more rapidly in new urban areas than in old urban areas. Both SUHI intensity and area demonstrated stronger growth during SDs compared to SNs. The method proposed in this paper produced satisfactory estimates of both LST and its trend, thereby laying a solid foundation for subsequent evaluation of how vegetation greenness changes affect LST and SUHI. Vegetation greenness changes were found to significantly increase both SUHI intensity and area. This effect is primarily attributed to vegetation greening in rural areas, which lowers rural LST and thereby enhances the urban-rural LST contrast. Vegetation greenness changes had a smaller impact on the trend in SUHI area than on SUHI intensity. This discrepancy can be attributed to the fact that urban core areas—already characterized by elevated LST—are consistently classified within the SUHI area irrespective of vegetation greenness changes.

In summary, this study provides a precise quantification of how urban and rural vegetation greenness changes affect both the intensity and area of SUHIs. However, to offer actionable suggestions for urban planning, future efforts should incorporate air temperature data to study the atmospheric UHI effect, along with knowledge of when the urban heat is exceeding thresholds that cause impacts. Additionally, future research should utilize model simulations to identify which vegetation biophysical properties (e.g., albedo and evapotranspiration) contribute most significantly to SUHI variations.

CRediT authorship contribution statement

Rui Yao: Writing – original draft, Software, Project administration, Methodology, Funding acquisition, Data curation, Conceptualization. **Zhihao Zhang:** Writing – review & editing, Software, Methodology, Data curation. **Wenjie Li:** Writing – review & editing, Software, Data curation. **Hao Li:** Writing – review & editing, Data curation. **Shiya Zhu:** Writing – review & editing, Data curation. **Hongji Zhu:** Writing – review & editing, Data curation. **Chuan Wang:** Writing – review & editing, Data curation. **Dewei Luo:** Writing – review & editing, Data curation. **Ying Yang:** Writing – review & editing, Data curation. **Junli Li:** Writing – review & editing, Methodology. **Weitao Han:** Writing – review & editing, Methodology. **Xin Huang:** Writing – review & editing, Supervision, Project administration, Funding acquisition.

Declaration of competing interest

The authors declare that they have no known competing financial interests or personal relationships that could have appeared to influence the work reported in this paper.

Acknowledgement

This research was funded by the Natural Science Foundation of Hubei Province of China (grant number 2025AFD075), National Natural Science Foundation of China (grant number 42507651), Natural Science Foundation of Hubei Province of China (grant number 2022CFD098) and the Doctoral Startup Foundation of Hubei University of Arts and Science (grant number QDF2024028).

Appendix A. Supplementary data

Supplementary data to this article can be found online at https://doi.org/10.1016/j.envres.2025.123423.

Data availability

Data will be made available on request.

References

Arnfield, A.J., 2003. Two decades of urban climate research: a review of turbulence, exchanges of energy and water, and the urban heat Island. Int. J. Climatol. 23, 1–26.
Blumstein, M., Webster, S., Hopkins, R., Basler, D., Yun, J., Marais, D.L.D., 2025. Genomics highlight an underestimation of phenology sensitivity to the urban heat island effect. Proc. Natl. Acad. Sci. U. S. A 122, e2408564122.
Chakraborty, T.C., Qian, Y., 2024. Urbanization exacerbates continental- to regional-scale warming. One Earth 7, 1387–1401.
Chen, C., Li, D., Keenan, T.F., 2021. Enhanced surface urban heat islands due to divergent urban-rural greening trends. Environ. Res. Lett. 16, 124071.
Cui, F., Hamdi, R., Yuan, X., He, H., Yang, T., Kuang, W., Termonia, P., De Maeyer, P., 2021. Quantifying the response of surface urban heat island to urban greening in global north megacities. Sci. Total Environ. 801, 149553.
Danielson, J.J., Gesch, D.B., 2011. Global multi-reC. solution terrain elevation data 2010 (GMTED2010). U.S. Geological Survey Open-File Report 2011–1073.
Donateo, A., Palusci, O., Pappaccogli, G., Esposito, A., Martilli, A., Santiago, J.L., Buccolieri, R., 2023. Analysis of urban heat island and human thermal comfort in a Mediterranean city: a case study of Lecce (Italy). Sustain. Cities Soc. 98, 104849.
Du, M., Li, N., Hu, T., Yang, Q., Chakraborty, T.C., Venter, Z., Yao, R., 2024. Daytime cooling efficiencies of urban trees derived from land surface temperature are much higher than those for air temperature. Environ. Res. Lett. 19, 044037.
Duan, S., Li, Z., Li, H., Göttsche, M., Wu, H., Zhao, W., Leng, P., Zhang, X., Coll, C., 2019. Validation of collection 6 MODIS land surface temperature product using in situ measurements. Rem. Sens. Environ. 225, 16–29.
Fang, Y., Du, X., Zhao, H., Hu, M., Xu, X., 2023. Assessment of green roofs' potential to improve the urban thermal environment: the case of Beijing. Environ. Res. 237, 116857.
Gui, X., Wang, L., Yao, R., Yu, D., Li, C., 2019. Investigating the urbanization process and its impact on vegetation change and urban heat island in Wuhan, China. Environ. Sci. Pollut. Control Ser. 26, 30808–30825.
Han, Y., Ge, H., Xu, Y., Zhuang, L., Wang, F., Gu, Q., Li, X., 2023. Estimating soil salinity using multiple spectral indexes and machine learning algorithm in Songnen Plain, China. IEEE J. Sel. Top. Appl. Earth Obs. Rem. Sens. 16, 7041–7050.

Hashemi, F., Mills, G., Poerschke, U., Iulo, L.D., Pavlak, G., Kalisperis, L., 2024. A novel parametric workflow for simulating urban heat island effects on residential building energy use: coupling local climate zones with the urban weather generator a case study of seven U.S. cities. Sustain. Cities Soc. 110, 105568.
Huete, A., Didan, K., Miura, T., Rodriguez, E.P., Gao, X., Ferreira, L.G., 2002. Overview of the radiometric and biophysical performance of the MODIS vegetation indices. Rem. Sens. Environ. 83, 195–213.
Imhoff, M.L., Zhang, P., Wolfe, R.E., Bounoua, L., 2010. Remote sensing of the urban heat island effect across biomes in the continental USA. Rem. Sens. Environ. 114, 504–513.
Islam, S., Karipot, A., Bhawar, R., Sinha, P., Kedia, S., Khare, M., 2024. Urban heat island effect in India: a review of current status, impact and mitigation strategies. Discover Cities 1, 34.
Jambhekar, R., Naidu, D.G.T., Krishnaswamy, J., 2025. Effects of heat stress and green cover on urban birds in the megacity of Bengaluru. Ecol. Appl. 35, e70039.
Kosaka, Y., Xie, S.-P., 2013. Recent global-warming hiatus tied to equatorial Pacific surface cooling. Nature 501, 403–407.
Kuhn, M., 2008. Building predictive models in R using the caret package. J. Stat. Software 28 (5), 1–26.
Kuhn, M., Quinlan, R., 2024. _Cubist: Rule- and instance-based regression modeling. R package version 0.4.4.
Lai, J., Zhan, W., Voogt, J., Quan, J., Huang, F., Zhou, J., Bechtel, B., Hu, L., Wang, K., Cao, C., Lee, X., 2021. Meteorological controls on daily variations of nighttime surface urban heat islands. Rem. Sens. Environ. 253, 112198.
Li, G., Cao, Y., Fang, C., Sun, S., Qi, W., Wang, Z., He, S., Yang, Z., 2024a. Global urban greening and its implication for urban heat mitigation. Proc. Natl. Acad. Sci. U. S. A 122, e2417179122.
Li, J., Li, G., Jiao, Y., Li, C., Yan, Q., 2024b. Association of neighborhood-level socioeconomic status and urban heat in China: evidence from Hangzhou. Environ. Res. 246, 118058.
Li, L., Zhan, W., Du, H., Lai, J., Wang, C., Fu, H., Huang, F., Liu, Z., Wang, C., Li, J., Jiang, L., Miao, S., 2022. Long-term and fine-scale surface urban heat Island dynamics revealed by landsat data since the 1980s: a comparison of four megacities in China. J. Geophys. Res. Atmos. 127 e2021JD035598.
Li, Y., Kong, X., Zhu, Z., 2020. Multiscale analysis of the correlation patterns between the urban population and construction land in China. Sustain. Cities Soc. 61, 102326.
Liu, H., He, B.-j., Gao, S., Zhan, Q., Yang, C., 2023a. Influence of non-urban reference delineation on trend estimate of surface urban heat island intensity: a comparison of seven methods. Rem. Sens. Environ. 296, 113735.
Liu, S., Shi, K., Wu, Y., Cui, Y., 2023b. Suburban greening and suburbanization changing surface urban heat island intensity in China. Build. Environ. 228, 109906.
Liu, Z., Li, J., Wu, Y., Qin, C., Liu, Y., 2025. Temporal trend of the frequency and maximum durations of surface urban heat islands over global cities. Sustain. Cities Soc. 120, 106141.
Lu, S., Liu, F., Ye, Y., Tang, J., Li, P., Lin, W., Guo, Y., Ma, R., Wang, J., 2024. Analysis of the spatio-temporal characteristics of Winter surface urban heat Island: a case Study in Beijing, China. J. Earth Sci. 35, 1640–1653.
Oke, T.R., 1973. City size and the urban heat ISLAND. Atmos. Environ. 7, 769–779.
Oke, T.R., Johnson, G.T., Styen, D.G., Watson, I.D., 1991. Simulation of surface urban heat islands under 'ideal' conditions at night part 2: diagnosis of causation. Boundary-Layer Meteorol. 56, 339–358.
Peng, S., Piao, S., Ciais, P., Friedlingstein, P., Ottle, C., Bréon, F.-M., Nan, H., Zhou, L., Myneni, R.B., 2011. Surface urban heat Island across 419 global big cities. Environ. Sci. Technol. 46, 696–703.
Quan, J., Chen, Y., Zhan, W., Wang, J., Voogt, J., Wang, M., 2014. Multi-temporal trajectory of the urban heat island centroid in Beijing, China based on a Gaussian volume model. Rem. Sens. Environ. 149, 33–46.
Quinlan, R., 1992. Learning with continuous classes. Proceedings of the 5th Australia Joint Conference on Artificial Intelligence. Hobart, Tasmania, pp. 343–348.
Raj, S., Yun, G.Y., 2024. Exploring the role of strategic urban planning and greening in decreasing surface urban heat island intensity. J. Asian Architect. Build Eng. 24, 866–879.
Rao, P., Torreggiani, D., Tassinari, P., Rötzer, T., Pauleit, S., Rahman, M.A., 2025. Do urban green spaces cool cities differently across latitudes? Spatial variability and climatic drivers of vegetation-induced cooling. Sustain. Cities Soc. 130, 106513.
Ren, Q., He, C., Huang, Q., Shi, P., Zhang, D., Güneralp, B., 2022. Impacts of urban expansion on natural habitats in global drylands. Nat. Sustain. 5, 869–878.
Robbiati, F.O., Cáceres, N., Hick, E.C., Suarez, M., Soto, S., Barea, G., Matoff, E., Galetto, L., Imhof, L., 2022. Vegetative and thermal performance of an extensive vegetated roof located in the urban heat island of a semiarid region. Build. Environ. 212, 108791.
Roshan, G., Sarli, R., Fitchett, J.M., 2022. Urban heat island and thermal comfort of Esfahan City (Iran) during COVID-19 lockdown. J. Clean. Prod. 352, 131498.
Schwarz, N., Lautenbach, S., Seppelt, R., 2011. Exploring indicators for quantifying surface urban heat islands of European cities with MODIS land surface temperatures. Rem. Sens. Environ. 115, 3175–3186.
Song, J., Przybysz, A., Zhu, C., 2025. Revealing the contribution of urban green spaces to improving the thermal environment under realistic stressors and their interactions. Sustain. Cities Soc. 126, 106426.
Song, X., Feng, Q., Xia, F., Li, X., Scheffran, J., 2021. Impacts of changing urban land-use structure on sustainable city growth in China: a population-density dynamics perspective. Habitat Int. 107, 102296.
Streutker, D.R., 2002. A remote sensing study of the urban heat island of Houston, Texas. Int. J. Rem. Sens. 23, 2595–2608.
Voogt, J.A., Oke, T.R., 2003. Thermal remote sensing of urban climates. Rem. Sens. Environ. 86, 370–384.
Wan, Z., 2014. New refinements and validation of the collection-6 MODIS land-surface temperature/emissivity product. Rem. Sens. Environ. 140, 36–45.
Wang, A., Dai, Y., Zhang, M., Chen, E., 2025. Exploring the cooling intensity of green cover on urban heat island: a case study of nine main urban districts in Chongqing. Sustain. Cities Soc. 124, 106299.
Wang, J., Huang, B., Fu, D., Atkinson, P.M., Zhang, X., 2016. Response of urban heat island to future urban expansion over the BeijingeTianjineHebei metropolitan area. Appl. Geogr. 70, 26–36.
Ward, K., Lauf, S., Kleinschmit, B., Endlicher, W., 2016. Heat waves and urban heat islands in Europe: a review of relevant drivers. Sci. Total Environ. 569–570, 527–539.
Wu, B., Zhang, Y., Wang, Y., He, Y., Wang, J., Wu, Y., Lin, X., Wu, S., 2024. Mitigation of urban heat island in China (2000–2020) through vegetation-induced cooling. Sustain. Cities Soc. 112, 105599.
Xu, D., Bai, T., Yang, L., Zhou, Y., Chen, B., Xu, H., Song, Y., Yuan, Y., Cui, Y., Meng, L., Xia, Z., Chen, M., Xu, Z., Zhao, P., Dong, G., Zhang, L., Zhao, J., Wu, W., Wang, W., Zhao, L., Cheng, J., Ciais, P., 2024. Quantifying the cooling effect of urban greening driven by ecological restoration projects in China. Environ. Sci. Technol. 58, 20990–21001.
Xu, Y., Knudby, A., Shen, Y., Liu, Y., 2018. Mapping monthly air temperature in the Tibetan Plateau from MODIS data based on machine learning methods. IEEE J. Sel. Top. Appl. Earth Obs. Rem. Sens. 11, 345–354.
Yang, C., Qin, Y., Wu, H., Zhao, Y., Che, S., 2025. Urban park green spaces and their potential in regulating urban heat Island (UHI) effects in urban-rural gradient in Shanghai, China. Sustain. Cities Soc. 129, 106467.
Yang, J., Huang, X., 2021. The 30 m annual land cover dataset and its dynamics in China from 1990 to 2019. Earth Syst. Sci. Data 13, 3907–3925.
Yang, M., Ren, C., Wang, H., Wang, J., Feng, Z., Kumar, P., Haghighat, F., Cao, S.-J., 2024. Mitigating urban heat island through neighboring rural land cover. Nature Cities 1, 522–532.
Yang, Q., Xu, Y., Tong, X., Huang, X., Liu, Y., Chakraborty, T.C., Xiao, C., Hu, T., 2023. An adaptive synchronous extraction (ASE) method for estimating intensity and footprint of surface urban heat islands: a case study of 254 North American cities. Rem. Sens. Environ. 297, 113777.
Yao, R., Huang, X., Zhang, Y., Wang, L., Li, J., Yang, Q., 2024. Estimation of the surface urban heat island intensity across 1031 global cities using the regression-modification-estimation (RME) method. J. Clean. Prod. 434, 140231.
Yao, R., Wang, L., Huang, X., Cao, Q., Wei, J., He, P., Wang, S., Wang, L., 2023a. Global seamless and high-resolution temperature dataset (GSHTD), 2001–2020. Rem. Sens. Environ. 286, 113422.
Yao, R., Wang, L., Huang, X., Gong, Wei., Xia, X., 2019. Greening in rural areas increases the surface urban heat island intensity. Geophysical Research Letters 46, 2204–2212.
Yao, R., Wang, L., Huang, X., Liu, Y., Niu, Z., Wang, S., Wang, L., 2021. Long-term trends of surface and canopy layer urban heat island intensity in 272 cities in the mainland of China. Sci. Total Environ. 772, 145607.
Yao, R., Wang, L., Huang, X., Niu, Y., Chen, Y., Niu, Z., 2018a. The influence of different data and method on estimating the surface urban heat island intensity. Ecol. Indic. 89, 45–55.
Yao, R., Wang, L., Huang, X., Zhang, W., Li, J., Niu, Z., 2018b. Interannual variations in surface urban heat island intensity and associated drivers in China. J. Environ. Manag. 222, 86–94.
Yao, R., Zhang, Y., Wang, L., Li, J., Yang, Q., 2023b. Reconstructed NDVI and EVI datasets in China (ReVIChina) generated by a spatial-interannual reconstruction method. International Journal of Digital Earth 16, 4749–4768.
Yuan, Y., Li, X., Wang, H., Geng, X., Gu, J., Fan, Z., Wang, X., Liao, C., 2024. Unraveling the global economic and mortality effects of rising urban heat island intensity. Sustain. Cities Soc. 116, 105902.
Zhang, J., Wang, Y., 2008. Study of the relationships between the spatial extent of surface urban heat Islands and urban characteristic factors based on landsat ETM+ data. Sensors (Basel) 8, 7453–7468.
Zhang, X., Friedl, M.A., Schaaf, C.B., Strahler, A.H., Schneider, A., 2004. The footprint of urban climates on vegetation phenology. Geophys. Res. Lett. 31, L12209.
Zhao, C., Pan, Y., Wu, H., Zhu, Y., 2024. Quantifying the contribution of industrial zones to urban heat islands: relevance and direct impact. Environ. Res. 240, 117594.
Zhao, Y., Li, R., Niu, J., Shi, X., Gao, N., 2025. Numerical simulation of diurnal and nocturnal impact of vegetated facades on microclimate. Build. Environ. 279, 113063.
Zhou, D., Xiao, J., Bonafoni, S., Berger, C., Deilami, K., Zhou, Y., Frolking, S., Yao, R., Qiao, Z., Sobrino, J., 2019. Satellite remote sensing of surface urban heat Islands: progress, challenges, and perspectives. Remote Sens. 11, 48.
Zhou, D., Xiao, J., Frolking, S., Zhang, L., Zhou, G., 2022. Urbanization contributes little to global warming but substantially intensifies local and regional land surface warming. Earths Future 10 e2021EF002401.
Zhou, D., Zhao, S., Zhang, L., Sun, G., Liu, Y., 2015. The footprint of urban heat island effect in China. Sci. Rep. 5, 11160.
Zhou, J., Chen, H.W., Li, H., Wang, Q., Wang, G., Jia, K., Chen, Z., Zhao, C., Shi, W., Yang, Y., Tang, Y., Chen, J., Zhang, Y., Xu, T., Wang, Y., Liu, G., Yan, X., 2025. Amplified urban heat island effect in southern china's old towns following atmospheric regulation policies. Sustain. Cities Soc. 131, 106675.